

# Nuclear conversion of $^{195}\text{AuFe}$ into $^{195}\text{PtFe}$ centers in silicon: observations by magnetic resonance

C.A.J. Ammerlaan<sup>a,\*</sup>, B.J. Pawlak<sup>a</sup>, ISOLDE Collaboration<sup>b</sup>

<sup>a</sup>*Van der Waals-Zeeman Institute, University of Amsterdam, Valckenierstraat 65, NL-1018 XE Amsterdam, Netherlands*

<sup>b</sup>*CERN, CH-1211 Geneva, Switzerland*

Received 9 September 2002; accepted 20 September 2002 by M. Grynberg

---

## Abstract

For the purposes of the reported experiments iron-doped silicon samples were implanted with nuclei  $^{195}\text{Hg}$ , which due to nuclear instability transmute via radioactive gold into stable platinum. Electron paramagnetic resonance was applied to monitor the conversion of  $^{195}\text{AuFe}$  centers into  $^{195}\text{PtFe}$  centers. On the basis of the hyperfine interactions both centers were unambiguously ascribed to gold and platinum impurities with mass 195, having their origin in the implantation. From the observation of centers with an equal geometrical structure, it is concluded that no atomic displacements due to recoil occur. Intensities of  $^{195}\text{AuFe}$  decrease with time and are accompanied by a simultaneous increase of  $^{195}\text{PtFe}$  signals, revealing the nuclear process. Deviation of the time dependence from the 183 days half-life of the  $^{195}\text{Au}$  isotope is ascribed to iron diffusion and to shift of the Fermi level in the samples during the center transformation. Accurately measured hyperfine interactions with the gold isotopes indicate a hyperfine structure anomaly of  $^{195}\text{Au}$  with respect to  $^{197}\text{Au}$  less than 1%.

© 2002 Elsevier Science Ltd. All rights reserved.

PACS: 61.72.Tt; 76.30.Fc; 76.30.He; 81.05.Cy

Keywords: A. Silicon; C. Impurities in semiconductors; D. Nuclear transmutation; E. Magnetic resonance

---

## 1. Introduction

The electronic properties of centers with deep electronic levels in the band gap of semiconductors are an important subject of study. From the point of view of fundamental materials science the understanding of the electronic structure of the centers is of great interest. Transition metals, with their inner d-shell electrons incorporated in elemental semiconductors, with host s and p electrons, represent a challenging case, requiring detailed experimental investigations of atomic and electronic properties and dedicated theoretical modeling.

Among such systems, the gold and platinum impurities in silicon have attracted intensive attention. Both platinum and gold are easily involved in complex formation with other impurities. Besides by magnetic resonance these processes have been followed by techniques such as photoluminescence and deep-level transient spectroscopy. The data have in general led to a consistent picture of these impurity reactions. A large number of complexes has been catalogued [1].

The main goal of the present investigation was the observation of a common origin shared by the centers with the consequent corollaries for their structures. In the experiment samples are prepared by the implantation of radioactive  $^{195}\text{Hg}$ . By the decay of this isotope, following the scheme  $^{195}\text{Hg}$  (10 h)  $\rightarrow$   $^{195}\text{Au}$  (183 d)  $\rightarrow$   $^{195}\text{Pt}$  (stable), gold and platinum centers are generated on a known time-scale. By electron paramagnetic resonance (EPR) the

---

\* Corresponding author. Tel.: +31-20-5255614; fax: +31-20-5255788.

E-mail address: ammerlaan@science.uva.nl (C.A.J. Ammerlaan).

gradual conversion of gold- into platinum-related centers, governed by the nuclear life-time, can be observed provided suitable conditions exist to form the centers in a paramagnetic state. A correlated decrease of the intensities of Au-related and increase of Pt-related spectra will provide direct evidence for a common origin of the centers. For the centers to have an equal geometrical structure it is required that the recoil energy released in the decay process does not induce atomic displacements.

The magnetic resonance spectrum with label Si-A23 was previously identified as arising from a Si:AuFe complex on the basis of resolved hyperfine interactions with both gold and iron [2]. The spectrum Pt(II) was assigned to platinum following the characteristic hyperfine pattern of the natural isotopes  $^{195}\text{Pt}$  and  $^{197}\text{Pt}$  [3], with a later demonstration of iron involvement [4]. Both complexes consist of a substitutional transition metal atom with an iron atom in a nearest interstitial site along a  $\langle 111 \rangle$  axis and thus have the trigonal symmetry. Spectroscopic parameters are well known [1].

## 2. Samples and experimental conditions

For the experiments float-zone silicon, n-type doped by phosphorus to the electrical resistivity of either  $5\ \Omega\ \text{cm}$  or  $125\ \Omega\ \text{cm}$ , was used. Flat samples with a thickness of  $0.35\ \text{mm}$  were implanted by mercury into a polished surface over an area of approximately  $25\ \text{mm}^2$ . Silicon materials of different resistivity were chosen to enhance the probability of producing the gold- and platinum-related centers in a paramagnetic state. Samples were implanted by  $^{195}\text{Hg}$  at the ISOLDE Division of CERN using the General Purpose Mass Separator. Two implantation energies, 30 and 60 keV, respectively, were used, with equal dose of  $8 \times 10^{12}$  atoms  $^{195}\text{Hg}$  for each energy per sample. Two different energies favor the more uniform distribution of implanted atoms. Computer simulation, by the TRIM program, shows that the implantation region is placed very shallow below the sample surface, typically in the layer between 15 and 45 nm in depth. The implantation volume is therefore estimated at  $0.75 \times 10^{-6}\ \text{cm}^3$  and the peak concentration of Hg at  $2 \times 10^{19}\ \text{cm}^{-3}$ . After around 3 days samples were thermally annealed at  $1000\ ^\circ\text{C}$  for 1 h, terminated by quench to room temperature. Annealing has the two beneficial effects of recrystallization of the surface layer of the sample and of broadening of the implanted impurity profile. By the broadening of the doped region the density of gold will be lowered with an enhanced possibility to produce isolated centers, rather than defect clusters. Presence of iron in the isolated atomic form is revealed by the associated EPR spectrum, with  $g = 2.0699$  [5]. Slow quenching promotes the formation of the trigonal AuFe pairs [2,6].

Magnetic resonance measurements were performed using a superheterodyne spectrometer with K-band micro-

wave frequency tuned to observe the dispersive part of the signal. For the EPR measurements samples were kept at the temperature 4.2 K. Measurements were made on both kinds of samples directly after thermal anneal. To follow the nuclear conversion the measurements were subsequently repeated with time intervals of 2 months. Due to their high level of radioactivity samples could only be stored at room temperature. In the low-resistivity samples the signal of neutral phosphorus was always present and served as an independent calibration of EPR intensity.

## 3. EPR results and analysis

### 3.1. EPR spectrum of the Si:AuFe pair

Measurements immediately following implantation and anneal show the well-known isotropic spectra of substitutional neutral phosphorus with  $g = 1.9985$  and of interstitial neutral iron at the  $g = 2.0699$  position. After approximately 6 months of sample storage at room temperature new resonances readily identifiable as the spectrum Si-A23 of the trigonal gold–iron impurity pair made their appearance. The spectrum as observed for magnetic field along a  $\langle 111 \rangle$  crystallographic direction is shown in Fig. 1. A fourfold splitting due to hyperfine interaction with a gold nucleus is apparent for the pair aligned along the field direction. The angular dependence of the spectrum follows the trigonal pattern as described in the literature for Si-A23 [2,6],

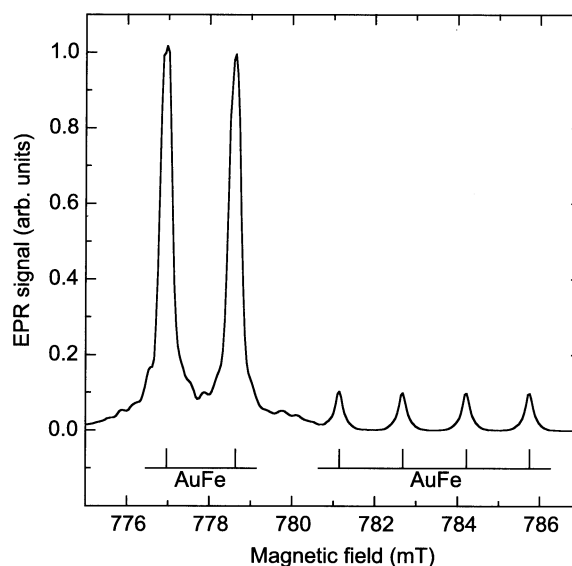


Fig. 1. EPR spectrum observed for the gold–iron pair in silicon, with magnetic field in a  $\langle 111 \rangle$  direction, microwave frequency  $\nu = 23.021684\ \text{GHz}$  and sample temperature  $T = 4.2\ \text{K}$ . At the higher fields the four nearly equidistant gold-hyperfine structure components of the pair oriented along the field direction are resolved, as indicated by the stick diagram.

Table 1  
Spin-Hamiltonian parameters of the  $^{197}\text{AuFe}$  and  $^{195}\text{AuFe}$  centers in silicon

Parameter	Center		Ratio ( $^{195}\text{Au}/^{197}\text{Au}$ )
	$^{197}\text{AuFe}$	$^{195}\text{AuFe}$	
$g_{\parallel}$	2.1001	2.0996	
$g_{\perp}$	2.1173	2.1169	
$g_n$	0.097164	0.09913	1.0203
$A_{\parallel}$ (MHz)	$45.06 \pm 0.15$	$45.70 \pm 0.06$	1.0143
$A_{\perp}$ (MHz)	$27.59 \pm 0.06$	$27.96 \pm 0.06$	1.0133
$a$ (MHz)	33.41	33.87	1.0137
$b$ (MHz)	5.82	5.91	1.0158

indicating equal Zeeman fine structure with the parameters as given in Table 1. Whereas in the published literature the prominent gold hyperfine interaction is for the  $^{197}\text{Au}$  isotope, in the present experiment the  $^{195}\text{Au}$  isotope will be present. As the nuclear properties of these isotopes are very similar the comparison of the spectra requires best accuracy. For the quantitative analysis the spin Hamiltonian

$$H = +\mu_B B g S - g_n \mu_N B I + S A I + I Q I, \quad (1)$$

with electron spin  $S = 1/2$  and nuclear spin  $I = 3/2$ , for both  $^{197}\text{Au}$  and  $^{195}\text{Au}$ , is appropriate. The Hamiltonian includes  $\langle 111 \rangle$ -axial tensors  $g$  for the Zeeman effect,  $A$  for the hyperfine interaction and  $Q$  for the quadrupole effect. Characterization of the gold impurity is by the hyperfine interaction. The principal value  $A_{\parallel}$  of the hyperfine interaction is most directly determined from the line

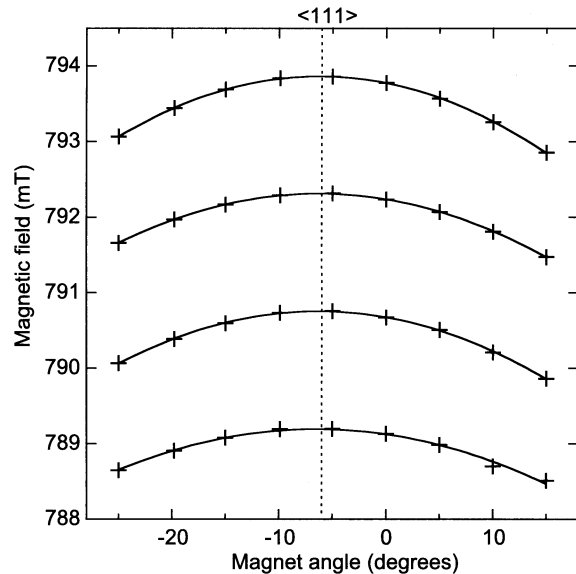


Fig. 2. Illustration of the parabolic fits made to the resonance fields of the radioactive gold–iron pair in an angular range from about  $-20^\circ$  to  $+20^\circ$  around the  $\langle 111 \rangle$  direction. Experimental data points are indicated by the + symbols.

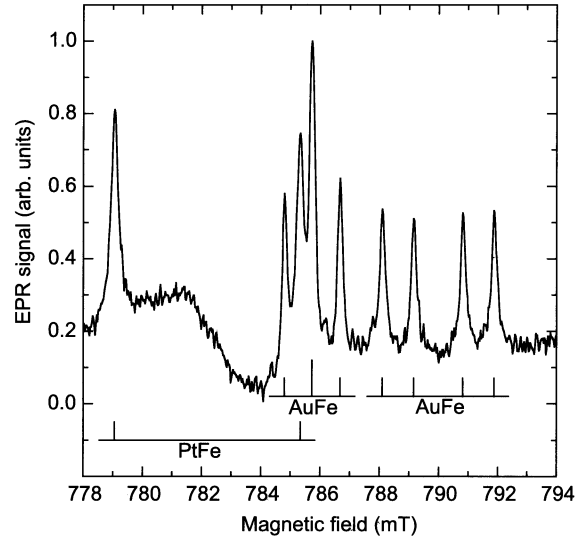


Fig. 3. EPR spectrum recorded 13 months after the implantation. Resonances from the AuFe and PtFe pairs are labeled by the stick diagrams. Resonances near 786 mT are from the AuFe centers with their axis perpendicular to the magnetic field. Measurement conditions: magnetic field parallel to  $\langle 011 \rangle$ , microwave frequency 23.28 GHz, sample temperature 4.2 K.

separations in the fourfold structure of the resonance for  $B \parallel \langle 111 \rangle$  for the defect oriented along the same axis. In this geometry the transitions are to high accuracy given by

$$h\nu = g_{\parallel} \mu_B B + A_{\parallel} m_I, \quad (2)$$

with  $m_I = -3/2, -1/2, +1/2$  and  $+3/2$ . For a best determination of the resonance field in the  $\langle 111 \rangle$  principal direction the signals as recorded over an angular range from  $-20^\circ$  to  $+20^\circ$  around the axial direction were fitted by parabolic curves, as shown in Fig. 2. Following the same procedure for samples of both the natural  $^{197}\text{Au}$ -doped and the  $^{195}\text{Au}$ -implanted silicon under identical conditions the direct comparison of hyperfine interactions with the two isotopes is made. Second-order corrections to the expression (2) are of order  $A_{\perp}^2 / g_{\parallel} \mu_B B \approx 30 \text{ kHz} \approx 1 \mu\text{T}$  and can be safely ignored as they are small, cancel when all transitions are taken into account, and, besides, are almost equal for the two isotopes. Results as given in Table 1 show slightly larger hyperfine interaction for the  $^{195}\text{Au}$  isotope, as expected. This serves as an identification of the  $^{195}\text{AuFe}$  complex introduced as a product of the implantation. The perpendicular principal value  $A_{\perp}$  manifests itself directly in the structure of the spectrum for  $B$  parallel to an  $\langle 011 \rangle$  direction, as shown in Fig. 3. Due to a large quadrupole effect the shape of the spectrum is quite special with two resonances coinciding at a central field and single lines separated from this position by  $+A_{\perp}$  and  $-A_{\perp}$  [2]. Resonance conditions are, respectively,

$$h\nu = g_{\perp} \mu_B B, \quad (3)$$

$$h\nu = g_{\perp} \mu_B B + A_{\perp} \quad (4)$$

and

$$h\nu = g_{\perp} \mu_B B - A_{\perp}. \quad (5)$$

The separation of the two outer lines allows the determination of  $A_{\perp}$  from these spectra and the comparison between the two isotopes. Spectra were recorded every  $5^{\circ}$  in an interval of  $\pm 20^{\circ}$  around  $\langle 011 \rangle$  and fitted with parabolic curves to obtain a best value for the perpendicular direction. The values obtained for  $A_{\perp}$ , given in Table 1, are very similar to the literature data and, showing an isotope effect, confirm the spectrum identification. However, in this  $\langle 011 \rangle$  case the determination is less accurate as the second-order corrections can be appreciable. These corrections depend on the quadrupole moment and, for instance, lead to a 4% underestimate for  $A_{\perp}$  when  $Q_{\parallel} = 20$  MHz. As the quadrupole moments of the two isotopes are different and the electric field gradient at the gold nucleus in the gold–iron pair is not known, the very precise comparison is prohibited.

### 3.2. EPR spectrum of the Si:PtFe pair

At larger times after the implantation a clear spectrum appeared which is identified as arising from the Si:PtFe pair. The spectrum, originally labeled Pt(II) [3], has been observed before and was shown to correspond to a well-characterized trigonal pair of substitutional platinum and interstitial iron. Due to a weak intensity of the signal and overlap with other resonances the entire angular dependence was difficult to follow. Good quality spectra could be recorded for the main directions  $\langle 111 \rangle$  and  $\langle 011 \rangle$ . The spectrum taken along the latter crystallographic direction is shown in Fig. 3. Line positions are analyzed with the Hamiltonian

$$H = +\mu_B B g S + S A I \quad (6)$$

with  $S = 1/2$  and  $I = 1/2$  for the nuclear spin of the  $^{195}\text{Pt}$  isotope. The quantitative identification of the center is based on the spectroscopic data for the perpendicular  $\langle 011 \rangle$  direction, which with  $g_{\perp} = 2.1265$  and  $A_{\perp} = 175$  MHz correspond to literature values [4]. A signal corresponding to the even-mass isotopes of platinum, all with nuclear spin  $I = 0$ , and total natural abundance of 66.2%, is absent. This confirms the origin of the observed PtFe pairs in the nuclear decay of parent  $^{195}\text{AuFe}$  centers.

### 3.3. Atom recoil

The consideration of changes of lattice site induced by the recoil energy is crucial in this kind of defect studies using radioactive species. As an example, in the decay  $^{105}\text{Ag}$  to  $^{105}\text{Pd}$  the recoil energy imparted to the Pd atom of 4.6 eV is equal to the cohesive energy of atoms in silicon. A change of lattice site is likely to occur. For the present system, the nuclear conversion  $^{195}\text{Au}$  to  $^{195}\text{Pt}$  is an electron capture

process with the emission of neutrino's and gamma particles. Recoil energies  $E_r = (E_{\nu\gamma})^2/2m_{\text{Pt}}c^2$  imparted to the Pt nucleus are less than 100 meV. For this small energy it is expected that the nuclear conversion process leaves the  $^{195}\text{Pt}$  atom on the original  $^{195}\text{Au}$  position. The observation in spin resonance of the two well-identified centers with an identical structure, i.e. a substitutional transition metal Au or Pt complexed with an interstitial Fe atom on a nearest-neighbor position in a  $\langle 111 \rangle$  direction, forms compelling support for this assumption. This conclusion provides basic knowledge for further studies using the nuclear decay method for gold/platinum-related centers of yet unknown structure.

### 3.4. Time dependence

As usual in these experiments with nuclear conversion of radioactive isotopes the evolution with time of impurity centers was monitored. In the first 6 months after implantation no centers created by the implantation were observed. Only after that incubation period the signals of AuFe and PtFe centers were detected. Apparently these centers were formed during storage of the samples at room temperature from iron present in the samples. Subsequently, the intensities of these signals were followed by repeating measurements in a 2-month time sequence. In agreement with the nuclear decay process an increase of platinum-related signal is observed at the expense of the signal from the gold center. The half-life  $\tau_{\text{Hg}} = 10$  h of implanted  $^{195}\text{Hg}$  is short compared to the half-life  $\tau_{\text{Au}} = 183$  days of the  $^{195}\text{Au}$  species. Under these conditions the gold and platinum concentrations are given in a good approximation, respectively, by

$$n_{\text{AuFe}}(t) = n_{\text{AuFe}}(0) \exp(-t/\tau_{\text{Au}}) \quad (7)$$

and

$$n_{\text{PtFe}}(t) = n_{\text{PtFe}}(\infty) [1 - \exp(-t/\tau_{\text{Au}})]. \quad (8)$$

As all gold is eventually transformed into platinum,  $n_{\text{PtFe}}(\infty) = n_{\text{AuFe}}(0)$ . The ratio of the EPR intensities  $I$  of the two centers should follow the expression

$$I_{\text{PtFe}}(t)/I_{\text{AuFe}}(t) = C [\exp(t/\tau_{\text{Au}}) - 1], \quad (9)$$

in which a constant  $C$  has been introduced to account for different sensitivities in observing the resonances. A best fit to the experimental data, shown by the curve in Fig. 4, is obtained by a time constant  $\tau = 156$  days. On one hand, this is close enough to the nuclear decay time  $\tau_{\text{Au}} = 183$  days to confirm that the nuclear transformation is indeed observed. On the other hand, the discrepancy indicates substantial interference with other time-dependent processes. One such process is the capture of iron by the gold and platinum impurities. Also the constant  $C$  might effectively change with time due to variation of the Fermi level when impurity reactions take place. It must be noted that the gold–iron complex is observed in the neutral state  $(\text{AuFe})^0$ , whereas

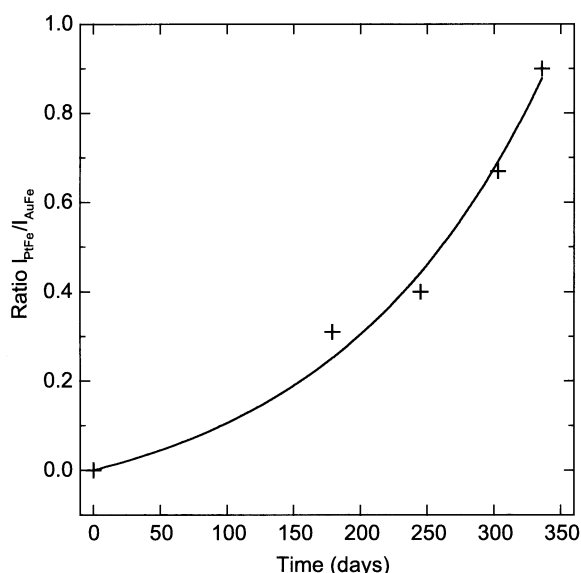


Fig. 4. Time evolution of the integrated EPR signal intensities of the AuFe and PtFe spectra. Solid curve represents a fit by the expression  $I_{\text{PtFe}}/I_{\text{AuFe}} = C[\exp(t/\tau) - 1]$  with the time constant  $\tau = 156$  days.

for PtFe an ionized state, probably  $(\text{PtFe})^-$ , is required. For AuFe electronic levels have been determined [7,8]; the corresponding information for the PtFe center is not available. An essential feature of these nuclear decay studies, when using techniques which are less specific for chemical identity, is to identify the elements involved by their lifetimes. Apparently, in the present kind of experiment such an argument has to be applied with care.

### 3.5. Hyperfine structure anomaly

Precise information on hyperfine interactions is required for the assessment of a possible anomaly. Inspection of Table 1 shows that the ratios obtained for the hyperfine constants  $A_{\parallel}$  and  $A_{\perp}$  of the 195 and 197 isotopes are slightly smaller than the ratio of their nuclear Zeeman factors  $g_n$ . For a proper analysis the hyperfine tensors are decomposed into their isotropic parts  $a$  and axially anisotropic parts  $b$ , using the transformations  $A_{\parallel} = a + 2b$  and  $A_{\perp} = a - b$ . A possible nuclear anomaly is related to parameter  $a$ , representing the Fermi contact interaction, but independent of  $b$ , which results from dipole–dipole interaction. Analysis shows that with  $b \approx 6$  MHz quite much smaller than  $a \approx 34$  MHz the effect of anisotropy parameter  $b$  on the anomaly can be almost ignored. This leads to the ratio  $^{195}a/^{197}a = 1.012$ . Following the traditional analysis, the hyperfine structure anomaly parameter  $^{195}\Delta^{197}$  is calculated from the definition

$$^{195}a/^{197}a = (^{195}g_n/^{197}g_n)(1 + ^{195}\Delta^{197}), \quad (10)$$

which, with  $^{195}g_n/^{197}g_n = 1.020$ , gives the value

$^{195}\Delta^{197} = -0.008$ . The small value indicates similar nuclear structure of the two isotopes. In contrast, larger hyperfine structure anomalies  $^{197}\Delta^{198} = +0.0853$  and  $^{197}\Delta^{199} = +0.037$  indicate a different distribution of magnetic moment in the mass 198 and mass 199 gold nuclei, respectively [9]. The hyperfine anomaly is accounted for in more detail by effects discussed by Bohr–Weisskopf and Breit–Rosenthal [10,11]. The present analysis is based on EPR measurements and provides limited accuracy. When samples with enhanced resonance signals become available a precise ENDOR experiment could improve the accuracy and substantiate the conclusion. Previous experiments on the  $^{121}\text{Sb}/^{123}\text{Sb}$  and on the  $^{47}\text{Ti}/^{49}\text{Ti}$  impurities in silicon have demonstrated the eminent suitability of ENDOR in the study of hyperfine structure anomalies [12,13].

## 4. Conclusion

The conversion by radioactive decay of paramagnetic centers has been observed for the  $\text{Au}_s\text{Fe}_i$  and  $\text{Pt}_s\text{Fe}_i$  impurity pairs in silicon. The origin of the centers as implantation products following the decay of the unstable  $^{195}\text{Hg}$  isotope was established independently for both species in the chain by the spectroscopic features. The paramagnetic resonance spectra confirm the identical geometrical atomic structure of the centers. No changes due to nuclear recoil occur. A small hyperfine structure anomaly between the  $^{195}\text{Au}$  and  $^{197}\text{Au}$  isotopes is suggested by the analysis of hyperfine interaction parameters. With the observation of the mass-195 isotopes the successful introduction of radioactive paramagnetic centers by the implantation is demonstrated, resulting in a monitoring of the decay processes by magnetic resonance.

## Acknowledgements

The authors are grateful for substantial contributions of various nature to M.O. Henry, M. Deicher, J. Bollmann, D. Forkel-Wirth, A. Burchard, T. Nilsson and M. Dietrich of the ISOLDE team. Support by the Stichting voor Fundamenteel Onderzoek der Materie (Foundation FOM) is gratefully acknowledged as well.

## References

- [1] C.A.J. Ammerlaan, Landolt-Börnstein: Numerical Data and Functional Relationships in Science and Technology, New Series, vol. III41A2α, Springer, Berlin, 2002, p. 244.
- [2] R.L. Kleinhenz, Y.H. Lee, J.W. Corbett, E.G. Sieverts, S.H. Muller, C.A.J. Ammerlaan, Phys. Stat. Sol. (b) 108 (1981) 363.
- [3] H.H. Woodbury, G.W. Ludwig, Phys. Rev. 126 (1962) 466.

- [4] A.B. van Oosten, N.T. Son, L.S. Vlasenko, C.A.J. Ammerlaan, *Mater. Sci. Forum* 38–41 (1989) 355.
- [5] G.W. Ludwig, H.H. Woodbury, R.O. Carlson, *Phys. Rev. Lett.* 1 (1958) 295.
- [6] M. Höhne, *Phys. Stat. Sol. (b)* 99 (1980) 651.
- [7] H. Lemke, *Phys. Stat. Sol. (a)* 75 (1983) 473.
- [8] S.D. Brotherton, P. Bradley, A. Gill, E.R. Weber, *J. Appl. Phys.* 55 (1984) 952.
- [9] P.A. vanden Bout, V.J. Ehlers, W.A. Nierenberg, H.A. Shugart, *Phys. Rev.* 158 (1967) 1078.
- [10] A. Bohr, V.F. Weisskopf, *Phys. Rev.* 77 (1950) 94.
- [11] J.E. Rosenthal, G. Breit, *Phys. Rev.* 41 (1932) 459.
- [12] J. Eisinger, G. Feher, *Phys. Rev.* 109 (1958) 1172.
- [13] D.A. van Wezep, C.A.J. Ammerlaan, *Phys. Rev. B* 37 (1988) 7268.